Molecular Cell, Vol. 8, 581–590, September, 2001, Copyright ©2001 by Cell Press

A Small Domain of CBP/p300 Binds Diverse Proteins: Solution Structure and Functional Studies

Charles H. Lin,[1,2] Brian J. Hare,[4,6] Gerhard Wagner,[4] Stephen C. Harrison,[1,3,4] Tom Maniatis,[1,5] and Ernest Fraenkel[1,7]

[1]Department of Molecular and Cellular Biology
[2]Department of Chemistry and Chemical Biology
[3]Howard Hughes Medical Institute
Harvard University
Cambridge, Massachusetts 02138
[4]Department of Biological Chemistry
and Molecular Pharmacology
Harvard Medical School
Boston, Massachusetts 02115

Summary

The transcriptional coactivators CBP and p300 are critical regulators of metazoan gene expression. They associate with many different DNA-bound transcription factors through small, conserved domains. We have identified a compactly folded 46 residue domain in CBP and p300, the IRF-3 binding domain (IBiD), and we have determined its structure by NMR. It has a helical framework containing an apparently flexible polyglutamine loop that participates in ligand binding. Spectroscopic data indicate that induced folding accompanies association of IBiD with its partners, which exhibit no evident sequence similarities. We demonstrate the significance both in vitro and in vivo of interactions between IBiD and a number of diverse partners. Thus, IBiD is an important contributor to signal integration by CBP and p300.

Introduction

Activation of gene expression in higher eukaryotes involves the ordered assembly of complex multicomponent protein machines comprising transcriptional activator and coactivator proteins, mediator complexes, general transcription factors, and RNA polymerase II. The functions of these complexes are to recognize and bind the enhancer/promoter, to remodel the surrounding chromatin, and to direct the basic transcription machinery to the start site of transcription. Transcriptional coactivators, which associate with promoters and enhancers primarily through protein-protein contacts, mediate interactions between DNA-bound transcription factors and the general transcription machinery. In addition, some have key roles in chromatin remodeling. Members of the CBP/p300 family of coactivators have been implicated in both processes (Goodman and Smolik, 2000; Janknecht and Hunter, 1996). Interactions between CBP/p300 and transcriptional activators are mediated by several small domains (Figure 1A), of which structures have been determined for only two, KIX (Radhakrishnan et al., 1997) and TAZ2 (De Guzman et al., 2000). CBP/p300 also contain an intrinsic acetyltransferase activity, which can modify histones as well as several transcription factors (Berger, 1999).

CBP/p300 participate in a wide range of cellular functions, including cell growth, differentiation, transformation, and apoptosis (Giles et al., 1998; Goodman and Smolik, 2000). In *D. melanogaster*, a mutation in the dCBP gene causes defective pattern formation during embryogenesis, and in *C. elegans*, inhibition of *cbp-1* expression causes hyperproliferation, developmental arrest, and loss of tissue specification in embryos. The human disease Rubinstein-Taybi Syndrome is caused by inactivation of a single CBP allele, which leads to severe developmental disorders. Similarly, in mice, inactivation of a single allele of either CBP or p300 also causes developmental defects, and homozygous inactivation leads to embryonic death. Thus, levels of CBP and p300 are limiting in the cell. The clinical importance of CBP/p300 is not limited to development. Several chromosomal translocations associated with hematologic malignancies have been shown to generate fusions of CBP/p300 with other proteins.

The functions of CBP/p300 can be studied to good advantage in the context of the well characterized human interferon-β (IFN-β) gene promoter. In response to virus infection, the bZIP proteins ATF-2 and c-jun, the interferon regulatory factors (IRFs) 3 and 7 and the NF-κB heterodimer p50/p65 are activated coordinately. Together with CBP/p300 and HMG-I(Y), they assemble into a large nucleoprotein complex called the IFN-β enhanceosome (reviewed in Maniatis et al., 1998). CBP/p300 serve as molecular connectors in the enhanceosome, contacting the transcription factors through distinct domains (Figure 1A). Of these contacts, the interaction between the transcriptional activator IRF-3 and CBP/p300 is of special interest. In virus-infected cells, IRF-3 and CBP/p300 associate in a high molecular weight protein complex called VAF (virus-activated factor), which is stable in the absence of the other enhanceosome components (Wathelet et al., 1998). In addition, the IRF-3-CBP interaction is important for coactivator-mediated localized histone hyperacetylation at the IFN-β promoter (Parekh and Maniatis, 1999).

We identify IBiD, a structural domain in the C-terminal region of CBP responsible for the interaction with IRF-3. In addition, we find that IBiD is sufficient for binding of CBP to Ets-2, the adenoviral oncoprotein E1A, the nuclear receptor coactivator (NCoA) protein TIF-2, and an IRF homolog encoded by the Kaposi's sarcoma-associated herpesvirus (KSHV IRF-1). Using heteronuclear NMR spectroscopy, we show that IBiD is compactly folded, and that it undergoes a structural transition on binding to partner proteins. We demonstrate that the structural integrity of IBiD is functionally important, and that competition for binding to IBiD is a possible mechanism by which viral gene products interfere with host gene transcription.

[5]Correspondence: maniatis@envoy.mcb.harvard.edu
[6]Present address: Vertex Pharmaceuticals, 130 Waverly Street, Cambridge, Massachusetts 02139.
[7]Present address: Whitehead Institute, Nine Cambridge Center, Cambridge, Massachusetts 02142.

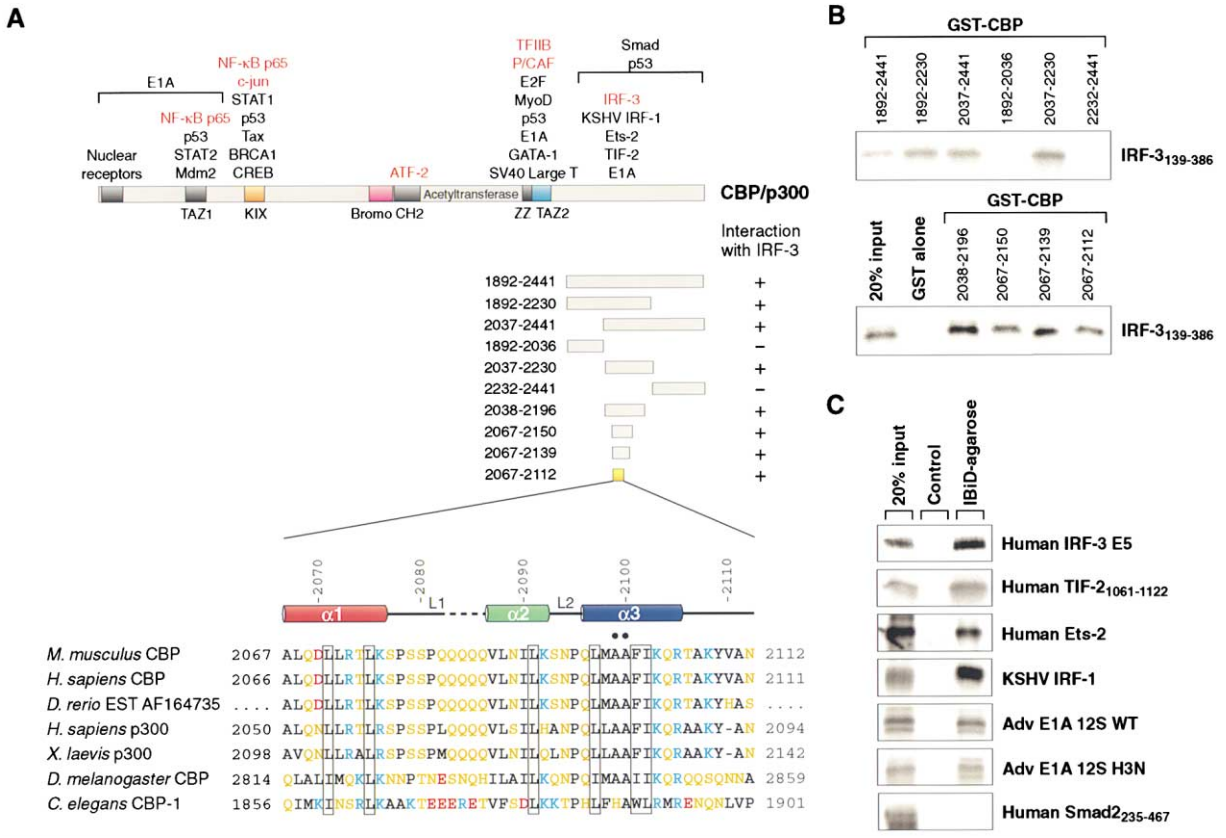

Figure 1. Identification of IBiD, a 46 Residue CBP Domain that Interacts with Multiple Proteins

(A) Diagram showing functional domains of mammalian CBP/p300 and a sequence alignment of all IBiD-related sequences from human CBP and p300, mouse CBP, *Xenopus* p300, *Drosophila* CBP, and *C. elegans* CBP-1. The sequence of a zebrafish EST corresponding to IBiD is also shown. In the overview of CBP/p300 domains, colored boxes indicate domains for which there are 3D structures. (The structure of the bromodomain is known from other proteins.) Selected interaction partners are listed; those involved in virus induction of IFN-β are labeled in red. In the sequence alignment, residues are colored based on amino acid type (acidic residues are red; basic, blue; polar, gold; nonpolar, black). The NMR-determined secondary structure of IBiD is indicated by the color-coded cylinders. The two black dots indicate the sites of Ala to Pro mutations (see Results). The least solvent-accessible residues are boxed. The four Gln residues indicated by a dashed line could not be assigned. A summary of the pull-down results in Figure 1B is also provided.

(B) In vitro pull-down assay testing for binding of IRF-$3_{139–386}$ to a series of CBP deletion mutants fused to GST.

(C) In vitro pull-down analysis using immobilized IBiD peptide showing binding of several nonhomologous proteins to IBiD.

Results

Identification of the IRF-3 Binding Domain in CBP

To map the minimal CBP domain required for IRF-3 interaction, we examined binding of IRF-3 to a series of CBP deletion mutants fused to glutathione S-transferase (GST). Prior to virus induction, the DNA binding, transactivation, and CBP interaction domains of IRF-3 are inhibited by intramolecular interaction involving the C terminus of the protein. Deleting residues at the C-terminal end or mutating a set of Ser/Thr residues to Glu or Asp makes IRF-3 constitutively active (Lin et al., 1998; Wathelet et al., 1998) (data not shown). We used a deletion mutant of human IRF-3, residues 139–386, in the GST pull-down assay. Residues 1892–2441 from the C-terminal transactivation region of mouse CBP bound well to IRF-$3_{139–386}$ (Figure 1B), consistent with previous observations (Kumar et al., 2000; Lin et al., 1998). To map the interaction in more detail, we generated an extensive series of CBP deletion mutants (Figure 1A). We found that 46 amino acids (residues 2067–2112) of the C-terminal region of CBP are sufficient for IRF-3 binding. We have named this domain IBiD.

Human and mouse CBPs have an identical IBiD sequence, and a zebrafish EST (GenBank accession number AF164735) is 96% identical. The corresponding sequences in human and *Xenopus* p300s are 80% and 78% identical to human CBP IBiD, respectively (Figure 1A). The differences between the human paralogs are mostly conserved amino acid substitutions. We also detected related sequences in *Drosophila* CBP and in *C. elegans* CBP-1 (see below).

IBiD Interacts with Nonhomologous Proteins

In addition to binding IRF-3, the C-terminal transactivation region of CBP/p300 has been reported to interact with many other proteins, including members of the NCoA/p160 family (Glass and Rosenfeld, 2000; Sheppard et al., 2001), members of the Ets family (Jayaraman et al., 1999; Papoutsopoulou and Janknecht, 2000), members of the Smad family (Feng et al., 1998; Janknecht et al., 1998), p53 (Van Orden et al., 1999), YY-1

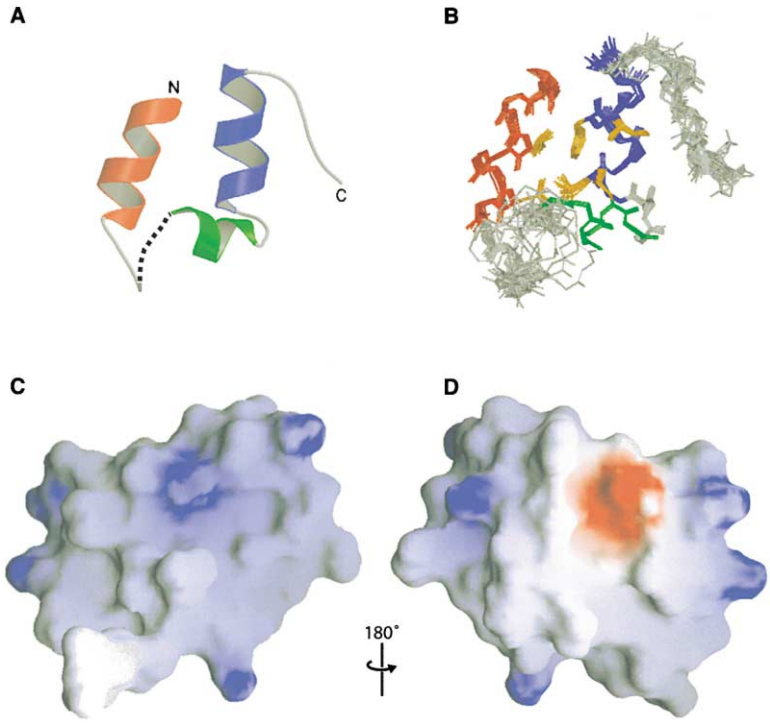

Figure 2. 3D Structure of IBiD

(A) A ribbon diagram showing the energy-minimized average structure of IBiD. The color of the helices matches those in Figure 1A. Four Gln residues (2083–2086) that could not be assigned are indicated by a dashed line.

(B) The ensemble of 12 structures of IBiD. Side chains of the solvent-inaccessible residues boxed in Figure 1A are shown in gold.

(C and D) Surface of the energy-minimized structure of IBiD colored by electrostatic potential. The orientation in (C) is the same as in Figures 2A and 2B; residues 2083–2086 are not shown. In (D) the molecule has been rotated by 180° about the vertical axis.

(Austen et al., 1997), human papillomavirus type 16 E6 protein (Patel et al., 1999), adenoviral E1A (Kurokawa et al., 1998), and KSHV IRF-1 (Burysek et al., 1999). To determine whether any of these proteins interacts with the C-terminal region through IBiD, we performed pull-down assays using immobilized IBiD peptide as bait. As shown in Figure 1C, a constitutively active mutant of IRF-3 (IRF-3 E5) (Falvo et al., 2000), Ets-2, KSHV IRF-1, the 12S isoform of E1A, and a fragment of TIF-2 containing the sequence required for CBP interaction all interacted specifically and directly with IBiD in vitro. In contrast, the MH2 domain of human Smad2 did not appear to interact with IBiD. Other candidate proteins remain to be tested. Using default parameters in BLAST, we did not detect any significant homology between IRF-3 and either Ets-2, TIF-2, or E1A. The only detectable homology between KSHV IRF-1 and IRF-3 is in the DNA binding domain, which is dispensable for the CBP interaction (Figure 1B). Thus, our data indicate that IBiD recognizes several proteins with no obvious sequence relationship.

Structure Determination

To study the structural basis for the function of IBiD, we expressed and purified from *E. coli* residues 2067–2112 of mouse CBP (2066–2111 of human CBP). Equilibrium ultracentrifugation and dynamic light-scattering measurements indicated that the purified protein was monomeric (data not shown), and circular dichroism spectra indicated it was predominantly α helical. Although this fragment failed to crystallize, 2D ^{1}H-^{1}H NOESY suggested that NMR could be used to determine the structure. Uniformly ^{13}C/^{15}N- and ^{15}N-labeled samples were prepared, and the structure was determined using multidimensional heteronuclear NMR techniques and simulated annealing. A superposition of 12 structures is shown in Figure 2B, and a summary of structural statistics is provided in Table 1.

The structure consists of three α helices that pack to enclose a hydrophobic core (Figures 2A and 2B). The residues between α1 and α2, labeled L1 (Figure 1A), contain a Ser/Pro-rich sequence, which forms an extended strand, and then a stretch of five Gln residues. Four of these Gln residues (2083–2086) could not be assigned, and two sets of backbone resonances were detected for some residues on either side of these amino acids. The observation of distinct sets of resonances is unusual and suggests the presence of two well-defined conformations, possibly due to isomerization of proline residues in L1. The structures were calculated using the stronger set of resonances. Residues 2087–2105 form two α helices (α2 and α3), which are separated by a 3 amino acid turn (L2) containing an invariant Pro. Thr2106 to Asn2112 form an extended strand that runs down the side of α3.

Helices α1 and α3 are roughly parallel and lie at right angles to α2. This "U" shaped space encloses six residues that are the most solvent inaccessible and form a small hydrophobic core (Leu2071, Leu2075, Leu2091, Leu2097, Phe2101, and Ile2102) (Figure 2B). These residues are identical in the vertebrate CBP/p300 sequences; in *Drosophila* CBP and *C. elegans* CBP-1 the corresponding positions show conservative substitutions (Figure 1A). The C-terminal tail partially covers a hydrophobic patch on α3, consisting of Met2098, Ala2099, and Ile2102. Overall, IBiD is highly positively charged with six basic residues and only one acidic amino acid (Figures 2C and 2D).

Significant Structural Changes Induced on Binding

One unusual feature of the IBiD structure is the presence of four Gln residues in L1 for which resonances could

Table 1. NMR Structure Determination Statistics	
NMR Restraints	
NOE restraints	
Total Unambiguous	724
Intraresidue	274
Sequential ($\|i-j\| = 1$)	167
Medium-range ($1 < \|i-j\| \leq 4$)	190
Long-range ($\|i-j\| > 4$)	93
Total ambiguous	108
Dihedral restraints	
ϕ	24
ψ	24
χ_1	10
NOE Violations	
Maximum individual violation	0.38 Å
Average violation	0.026 ± 0.0037 Å
Deviations from Ideal Geometry	
Bond length	0.0037 ± 0.00024 Å
Bond angles	0.72 ± 0.027°
Improper angles	0.64 ± 0.037°
RMS Deviation from Mean Structure	
Helices only	
Backbone	0.20 Å
Heavy atoms	0.51 Å
All residues	
Backbone	1.5 Å
Heavy atoms	2.0 Å

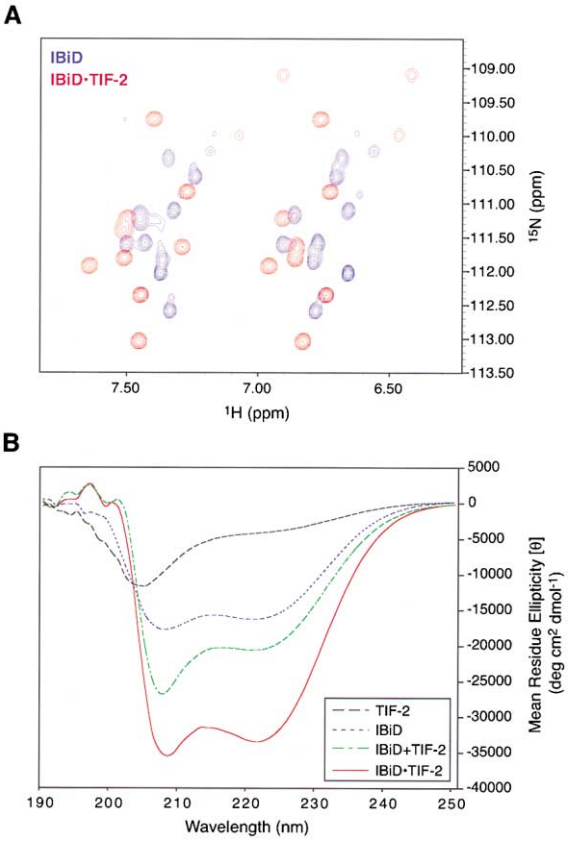

Figure 3. Evidence for Induced Structure

(A) The side chain amide region from ^{1}H-^{15}N HSQC spectra of ^{15}N-labeled IBiD alone (blue) and in the presence of equimolar TIF-$2_{1061–1108}$ (red).

(B) Circular dichroism spectra for IBiD and TIF-$2_{1061–1108}$. The spectrum taken with both proteins in the light path but unmixed is a dashed green line (IBiD + TIF-2). The spectrum taken after allowing the two proteins to mix is a solid red line (IBiD·TIF-2).

not be assigned but which are required for high-affinity binding of CBP to the TIF-2 homolog SRC-1 (Sheppard et al., 2001). To explore the possibility that these residues might undergo a structural change on binding to partner proteins, we measured the HSQC spectra of ^{15}N-labeled IBiD in the presence and absence of unlabeled TIF-$2_{1061–1108}$. These peptides form a 1:1 complex in a native polyacrylamide gel electrophoresis (PAGE) assay (data not shown). In these spectra, each amide proton gives rise to a single resonance peak. Many resonances change in the complex, suggesting an extensive interface between the two proteins. In particular, the side chain amides show a significant increase in dispersion in the presence of TIF-2 (Figure 3A). Because L1 contains 5 of the 11 Gln/Asn residues in IBiD, these data demonstrate increased order of L1 in the complex. Circular dichroism (CD) spectra also provide evidence that a structural transition occurs upon binding. The spectrum of IBiD is consistent with its α-helical fold (Figure 3B). The TIF-2 peptide alone shows little evidence of secondary structure. Mixing the two peptides causes a dramatic increase in helical signal. The molar ellipticity at 222 nm can be used to estimate roughly the fraction of a protein that is helical (Deleage and Geourjon, 1993). On the basis of this calculation, IBiD is 43% helical and TIF-2 is 11% helical, whereas the complex is 89% helical. These results demonstrate that binding induces folding in both TIF-2 and IBiD.

The Structural Integrity of IBiD Is Required for Virus Induction of IFN-β

The NMR data suggest that mutating the highly conserved residues Ala2099 and Ala2100 to Pro might cause IBiD to lose its structural integrity by disrupting α3 and removing the hydrophobic contribution of the two conserved Phe2101 and Ile2102 side chains. Indeed, the mutant (AAPP) failed to form a complex with TIF-$2_{1061–1108}$ in a native PAGE assay (data not shown). Therefore, we fused wild-type (wt) and mutant IBiD, separately, to the DNA binding domain of Gal4 and tested the chimeras in cotransfection experiments using a promoter containing five copies of Gal4 binding sites (Figure 4A). Gal4-IBiD showed an increase in activity upon Sendai virus infection, presumably because endogenous, phosphorylated IRF-3 was recruited to the promoter by IBiD to transactivate gene expression. Overexpression of IRF-3 significantly enhanced the response to virus, and the basal level was also slightly increased. In contrast, Gal4-IBiD AAPP did not show any virus-dependent response, even when IRF-3 was overexpressed, suggesting that the mutant IBiD is not functional in transcriptional activator recruitment. Overexpression of TIF-2 also led to an increase in Gal4-IBiD-driven transcription (Figure 4A), consistent with the proposal that CBP and p/CIP, another NCoA protein, are constitutively associated (Torchia et al., 1997). The AAPP mutant did not respond to

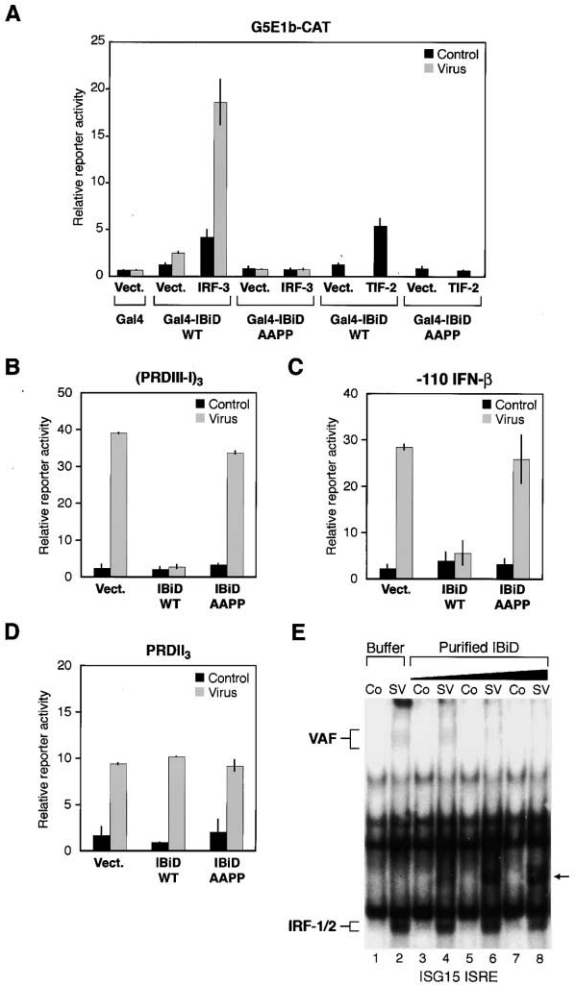

Figure 4. Structural Integrity of IBiD Is Required for Virus Induction of IFN-β and Assembly of VAF

(A) CAT assays showing the transcriptional activity of wild-type (WT) or mutant (AAPP) Gal4-IBiD in response to IRF-3 or TIF-2 overexpression. For each experiment, 500 ng of reporter and 50 ng of Gal4 construct were cotransfected with vector, IRF-3 (400 ng), or TIF-2 (1 μg). The full-length IRF-3 and TIF-2 constructs have been described (Voegel et al., 1998; Wathelet et al., 1998). Reporter activity shown in this and subsequent figures is the average of three experiments; error bars indicate ±1 standard deviation.

(B–D) CAT assays showing virus induction levels measured in extracts of cells transfected with either vector alone or WT or mutant IBiD. Experiments were conducted with the following reporter constructs: $(PRDIII\text{-}I)_3$-CAT contains three copies of the IRF-dependent element of the IFN-β enhancer (B); −110 IFN-β-CAT contains nucleotides −110 to +22 of the human IFN-β gene (C); $PRDII_3$-CAT contains three copies of the NF-κB-dependent element of the IFN-β enhancer (D).

(E) EMSAs showing the disruption of VAF caused by IBiD peptide and formation of a new complex (indicated by an arrow). Whole-cell extracts (WCEs) were prepared either from control HEC-1B cells (Co) or cells infected with Sendai virus for 6 hr (SV). WCEs were preincubated with either buffer alone (lanes 1 and 2) or increasing amounts of purified IBiD peptide (lanes 3 and 4, 100 nM final; lanes 5 and 6, 300 nM; lanes 7 and 8, 1 μM) for 10 min before the addition of ^{32}P-labeled ISG15 ISRE, a high-affinity VAF binding site (Wathelet et al., 1998). Protein-DNA complexes indicative of IRF-1 and IRF-2 binding were also observed, but their intensities were not affected by IBiD. Unbound DNA is not shown.

TIF-2 overexpression. We conclude that the protein-protein interactions mediated by IBiD are important for recruitment of CBP by transcriptional activators/coactivators, and that these interactions depend on a stable, properly folded IBiD structure.

Next, we sought evidence for the role of IBiD in virus induction of the IFN-β gene. If overexpressed, can IBiD have a dominant-negative effect by outcompeting endogenous CBP/p300 for binding to IRF-3? Indeed, IBiD strongly inhibited virus induction of reporter constructs bearing either the IFN-β promoter (−110) or three copies of PRDIII-I, the IRF-dependent element of the IFN-β enhancer (Figures 4B and 4C). In contrast, IBiD had no effect on activation of PRDII, a virus-inducible element that depends on NF-κB binding (Figure 4D). Because NF-κB contacts CBP through a different region (Figure 1A), this result indicates that the inhibition was specific and not due to dominant-negative effects on interactions between CBP and the general transcription machinery. Overexpression of mutant IBiD had little effect on virus induction of PRDIII-I or the IFN-β promoter (Figures 4B and 4C), confirming the requirement for a stable IBiD structure. Both transfected IBiD constructs were expressed in the cell line used, as detected by immunoblot analysis (data not shown). Taken together, these data demonstrate that IBiD participates in IFN-β gene activation in vivo.

The simplest explanation for the inhibitory effect of IBiD on IFN-β expression is that transfected IBiD associates with endogenous, phosphorylated IRF-3, preventing formation of VAF. As a consequence, a functional IFN-β enhanceosome cannot assemble. To strengthen this argument, we examined the effect of IBiD on the VAF complex in electrophoretic mobility shift assays (EMSAs). Increasing amounts of IBiD peptide specifically eliminated VAF (Figure 4E). In addition, a new, rapidly migrating DNA binding activity appeared. The new complex contained IBiD and the DNA binding subunits of VAF but not endogenous CBP or p300, as confirmed using specific antibodies (data not shown). Formation of the new complex in vivo was not sufficient for normal levels of virus induction (Figures 4B and 4C), strongly suggesting that full-length CBP/p300 are essential transcriptional coactivators and molecular connectors in the cooperative assembly of a functional IFN-β enhanceosome. We conclude that IBiD is a functionally important domain of CBP and that its structural integrity is required for its functions.

Competition for IBiD Binding as a Mechanism for Viral Intervention

To understand the significance of the multiple interactions with IBiD deduced from data in Figure 1C, we performed a series of in vivo experiments using Gal4-TIF-$2_{1041–1122}$. Alone, Gal4-TIF-$2_{1041–1122}$ increased transcription of the reporter, presumably by recruiting endogenous CBP/p300 to the promoter (Voegel et al., 1998). Cotransfection of E1A led to a significant decrease in reporter activity, consistent with the observation that binding of E1A to the C-terminal transactivation region of CBP prevents both formation of the p/CIP-CBP complex and activation of RAR-dependent pathways (Kurokawa et al., 1998).

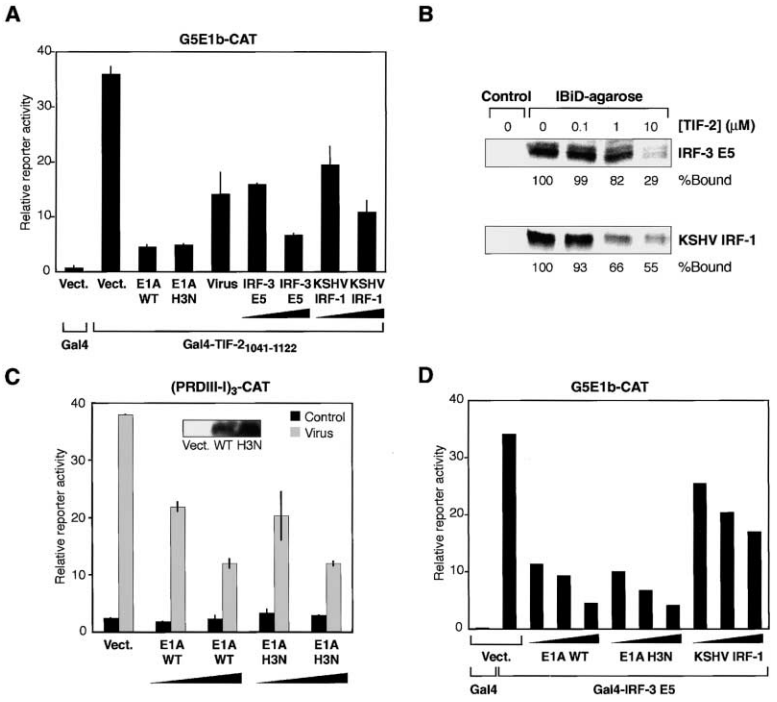

Figure 5. IRF-3, KSHV IRF-1, TIF-2, and E1A Compete for Binding to IBiD

(A) CAT reporter activity measured in extracts of cells transfected with the indicated plasmids (E1A 12S WT or H3N: 1 μg; IRF-3 E5: 0.5 μg and 1 μg; KSHV IRF-1: 0.5 μg and 1 μg) or infected with Sendai virus.

(B) In vitro pull-down analysis using immobilized IBiD showing the competition for binding to IBiD between TIF-2 (cold) and either IRF-3 E5 or KSHV IRF-1 (^{35}S-labeled). The percentages of IRF-3 E5 and KSHV IRF-1 that remained bound are shown.

(C) CAT assays showing the inhibitory effect of either WT or H3N E1A 12S on virus induction of $(PRDIII\text{-}I)_3$. Amounts of effector constructs transfected: 0.5 and 1 μg. Immunoblot analysis (inset) using an α-E1A antibody (Santa Cruz) indicates the expression levels of these E1A constructs.

(D) CAT assays showing the inhibitory effect of either WT or H3N E1A 12S, and KSHV IRF-1 on the transcription driven by Gal4-IRF-3 E5. Amounts of effector constructs transfected: Gal4-IRF-3 E5, 50 ng; viral gene constructs, 0.25, 0.5, and 1 μg.

In virus-infected cells, the activity of Gal4-TIF-$2_{1041–1122}$ was significantly lower than in mock-infected cells. Because virus infection causes essentially all IRF-3 molecules in the cell to associate with CBP/p300 (Wathelet et al., 1998), endogenous, phosphorylated IRF-3 may compete with Gal4-TIF-$2_{1041–1122}$ for their common site on CBP. To test whether this competition occurs, we cotransfected the IRF-3 E5 mutant and observed a dose-dependent reduction in the activity of Gal4-TIF-$2_{1041–1122}$ (Figure 5A). We obtained similar results by cotransfecting KSHV IRF-1. To determine if the antagonism between TIF-2, IRF-3, and KSHV IRF-1 involved IBiD, we performed an in vitro pull-down assay using TIF-$2_{1061–1108}$ as a competitor. Increasing amounts of TIF-2 peptide displaced either IRF-3 E5 or KSHV IRF-1 from immobilized IBiD (Figure 5B). In summary, our data show that IRF-3, KSHV IRF-1, and TIF-2 compete with each other for binding to IBiD.

E1A inhibits IFN-β expression (Ackrill et al., 1991) and contacts CBP through multiple sites (Figure 1A). To determine whether this inhibition involves competition with IRF-3 for binding IBiD, we examined the effect of E1A on virus induction of PRDIII-I. Overexpression of E1A suppressed the activity of PRDIII-I significantly (Figure 5C). To rule out the possibility that E1A inhibits IFN-β expression by disrupting the TAZ2-dependent CBP-RNA polymerase II holoenzyme interaction (Nakajima et al., 1997), we used a mutant (H3N) of E1A that is defective for interaction with TAZ2 (Kurokawa et al., 1998) and found that it inhibited PRDIII-I activity to a similar extent. In another experiment, we examined the transcriptional activity of Gal4-IRF-3 E5. This construct is highly active in the absence of virus infection due to its constant association with CBP/p300. Both wt and mutant E1As inhibited Gal4-IRF-3 E5 to similar extents and in a dose-dependent manner. The two sets of cotransfection experiments in Figures 5C and 5D are specific for the IRF-3-dependent pathway. These experiments, together with our observation that both wt and mutant E1As interact with IBiD in vitro (Figure 1C), strongly suggest that E1A inhibition of IFN-β expression involves competition with IRF-3 for binding to IBiD. Our results also indicate that KSHV IRF-1 interferes with IFN-β expression, at least in part, by targeting the IRF-3-IBiD interaction (Figures 1C and 5D).

Discussion

IBiD, the domain of CBP we have identified and studied, is required for interactions with IRF-3, TIF-2, Ets-2, E1A, and KSHV IRF-1. These proteins contribute to diverse cellular pathways. IRF-3 has an essential role in innate immunity due to its participation in the transcriptional activation of type I IFNs, RANTES, and several other antiviral genes (Mamane et al., 1999). TIF-2 belongs to a family of transcriptional coactivators (NCoA/p160) involved primarily in nuclear receptor dependent pathways (Glass and Rosenfeld, 2000). Ets-2 belongs to a large family of transcription factors (Ets) that affect cellular functions such as proliferation, differentiation, and lymphocyte and skeletal development (Sementchenko and Watson, 2000). Adenoviral E1A interferes with normal cellular transcription and cell cycle progression (Hottiger and Nabel, 2000). KSHV IRF-1 interferes with type I IFN expression, and its presence has been correlated with aberrant cell proliferation (Burysek et al., 1999; Nguyen et al., 1997). We do not yet understand the specificity determinants that allow IBiD to bind to these various proteins, which lack any obvious sequence homology.

Our CD data indicate that TIF-2 undergoes significant folding on binding IBiD. In addition, the HSQC spectrum

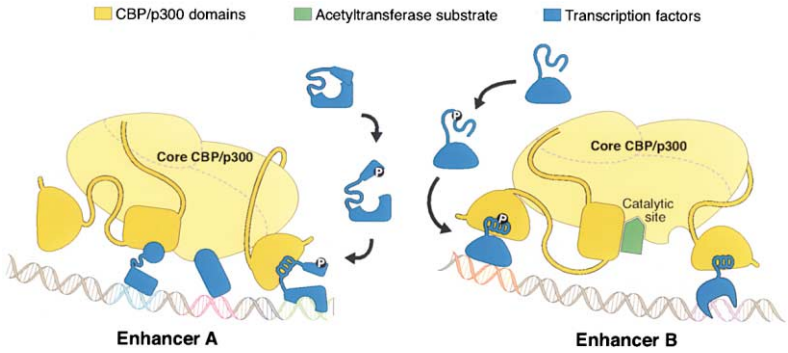

Figure 6. Flexible Domain Organization of CBP/p300

Schematic diagram illustrating how flexible tethers may permit CBP/p300 molecules to adapt to different enhancers. Binding of ligands can indirectly modify acetyltransferase activity by causing domain rearrangements. Two mechanisms by which phosphorylation of a ligand regulates its binding to CBP/p300 are also shown.

of ^{15}N-labeled IBiD in the presence of unlabeled TIF-2 provides direct evidence that Gln residues in L1, which are not defined in the NMR structure, have an altered conformation in the complex. Such "contingent folding" (Lei et al., 2000) has been observed with other activation domains including CREB (Radhakrishnan et al., 1997), VP16 (Uesugi et al., 1997), and p53 (Kussie et al., 1996).

CBP/p300 and Signal Integration

IBiD, KIX, and TAZ2 are the only domains of CBP that have been characterized structurally (the structures of bromodomains from other proteins are also known). Although IBiD, KIX, and TAZ2 are structurally distinct, they share the ability to bind diverse proteins with little sequence homology. The KIX domain accomplishes this promiscuity by recognizing an amphipathic α helix, and TAZ2 has been shown to bind a p53 peptide that can adopt an α-helical fold (De Guzman et al., 2000). It is possible that IBiD also recognizes a short structural motif.

Binding of CREB to KIX requires direct recognition of a phosphorylated Ser residue (Parker et al., 1998; Radhakrishnan et al., 1997), whereas binding of c-Myb is phosphorylation independent (Parker et al., 1999). Although binding of intact IRF-3 to IBiD requires phosphorylation of several Ser/Thr residues at the C-terminal end of IRF-3 (positions 396, 398, 402, 404, and 405) (Lin et al., 1998), those phosphorylated residues are not involved in making IBiD-IRF-3 contacts (Figure 1B). Of the remaining IBiD ligands we have identified, TIF-2, Ets-2, KSHV IRF-1, and E1A do not appear to require posttranslational modification for binding (Figures 1C and 5B). The viral proteins E1A and KSHV IRF-1 are, of course, present only after adenoviral and herpesviral infections, respectively. Thus, a variety of signals, including expression levels and posttranslational modifications, regulate ligand binding to CBP.

As the various combinations of ligands (activators, coactivators, etc.) recruit CBP to different promoters, CBP in turn integrates the signals and provides a complex logical readout. Signal integration can occur by at least two mechanisms. Docking of CBP or p300 into an enhanceosome by multiple, relatively weak contacts between different CBP/p300 domains and different DNA-bound activators (or activator-associated coactivators) can produce a series of logical "AND" operations, requiring active forms of most or all of the correct transcription factors. For example, both NF-κB and IRF-3 must be activated and present in the nucleus for expression of IFN-β. Competition among different factors for the same site can produce "NOT" and "OR" decisions, and viruses can intervene by elaborating their own CBP ligands.

Domain Organization and Adaptability of CBP/p300

The requirement for CBP to function at many different enhancers presents a structural puzzle. How can CBP form stable complexes at these diverse sites when each enhancer presents CBP ligands in different positions and orientations? A possible explanation emerges from analysis of distantly related CBP/p300 sequences. Using pairwise BLAST we have found that besides the core region (Bromo-CH2-acetyltransferase-ZZ-TAZ2) (Figure 1) (Bordoli et al., 2001), only TAZ1, KIX, and IBiD are conserved between human and *Drosophila* CBPs. In both organisms the sequences on either side of the core contain long, degenerate stretches of amino acids that vary both in length and composition. These sequences are unlikely to adopt a stable fold. The 440 amino acids between KIX and the core are Pro-rich in humans, whereas in *Drosophila* the corresponding region is over 700 amino acids long and is rich in Gln, Ser, and Gly. Similarly, the region between the core and IBiD is Gln/Pro-rich in humans, whereas in *Drosophila* the sequence is 50% longer and Gly-rich.

Although many transcription factors contain some disordered regions, almost half of human CBP/p300 and two-thirds of *Drosophila* CBP are likely to lack a well defined structure. These sequences presumably serve as loose tethers that covalently link CBP domains yet allow them sufficient freedom in position and orientation to function at diverse enhancers (Figure 6). This long range flexibility helps explain why insertion of a full helical turn of DNA between transcription factor binding sites in the IFN-β enhancer does not affect the level of virus induction (Thanos and Maniatis, 1995). The flexibility of CBP is limited, however, because a half turn insertion between transcription factor binding sites or an artificial activation surface produced by domain swapping is not tolerated (Merika et al., 1998).

The apparent flexibility in CBP quarternary structure may also help regulate its enzymatic activity. KSHV IRF-1 (Li et al., 2000) and a fragment of the TIF-2 homolog p/CIP (Perissi et al., 1999) can alter CBP/p300 acetyltransferase activity, even though the catalytic domain is located over 300 residues away from IBiD (Figure 1).

Binding of these ligands may induce rearrangements of the CBP domains that influence the activity of the catalytic core. Such a situation would be similar to that of Src-kinase, where activity is regulated by intramolecular interactions involving the SH2, SH3, and catalytic domains (Xu et al., 1999).

Conclusion

We have identified a conserved domain in the C-terminal transactivation region of CBP/p300. IBiD is small, yet it folds without stabilization by a metal ion or disulfide bond, placing it in an unusual category of proteins known as minidomains (McKnight et al., 1997; Spector et al., 1999). IBiD-dependent interactions are eliminated, in vitro and in vivo, by mutations that destabilize its structure. Nevertheless, binding involves contingent folding. Further structural work will allow us to understand the basis for specificity in IBiD interactions with the diverse partners and to see how these contacts alter the structure and function of CBP/p300.

Experimental Procedures

Plasmid Constructs and Sequence Analysis

Effector constructs for transient transfections and in vitro translation were cloned into pcDNA vectors. Reporter constructs have been described (Wathelet et al., 1998). Ets-2 and Smad2 were PCR amplified from a human cDNA library (Stratagene, La Jolla, CA). IBiD AAPP was generated by PCR mutagenesis. Constructs assembled from PCR fragments were verified by sequencing. CBP sequences were analyzed using Profilescan (http://www.isrec.isb-sib.ch) (Bucher et al., 1996).

Protein Expression and Purification

IBiD was overexpressed in *E. coli* BL21(DE3) with an N-terminal His_6 tag. Soluble protein was purified using Ni-NTA resin, and the tag was removed by TEV protease (Life Technologies, Carlsbad, CA), leaving four nonnative amino acids at the N terminus. IBiD was purified to homogeneity by reversed phase HPLC (RP-HPLC) and verified by electrospray ionization mass spectrometry (ESI-MS). Bacteria used to prepare NMR samples were grown in M9 media containing ^{13}C-D-glucose and/or ^{15}N-NH_4Cl. Human TIF-$2_{1061–1108}$ was prepared by solid phase synthesis on an ABI 431A synthesizer, RP-HPLC-purified, and verified by ESI-MS.

NMR Spectroscopy

Spectra were collected at 25°C. Sequential assignment of the backbone was determined using HNCA, HNCOCA, HNCACB, and HNCO CACB spectra (500 MHz INOVA). Side chains were assigned using ^{15}N-edited TOCSY, HCCONH, and CCONH spectra (500 MHz INOVA). χ_1 angles and stereospecific assignment of β-methylene protons were determined using HNHB (Archer et al., 1991) and 30 ms ^{15}N-TOCSY-HSQC (Clore et al., 1991) experiments (500 MHz Varian). A ^{1}H-^{13}C HSQC spectrum of 10% ^{13}C-labeled IBiD (600 MHz Brucker) was used to assign Leu and Val methyl protons (Szyperski et al., 1992).

Three NOESY spectra were used to determine distance constraints: a ^{13}C-edited NOESY (80 ms mixing time; 500 MHz), a ^{15}N-edited NOESY (150 ms mixing time; 500 MHz) and a ^{1}H-^{1}H NOESY (120 ms mixing time; 750 MHz Varian). Twenty-four pairs of ϕ and ψ were restrained using values predicted by TALOS (Cornilescu et al., 1999) with a reliability score ≥9. Spectra were processed in Felix97 (Molecular Simulations). Peaks were assigned and integrated using XEASY (Bartels et al., 1995). ^{1}H-^{15}N HSQC spectra of ^{15}N-labeled IBiD were recorded on a 500 MHz Unity spectrometer.

Structure Determination

Integrated peak lists, chemical shift tables, and dihedral constraints (Table 1) were used as input to ARIA (Nilges and O'Donoghue, 1998) linked to CNS (Brunger et al., 1998). Eight rounds of torsion angle simulated annealing were carried out. In each round, the lowest energy structures were used to automatically calibrate the spectra and determine assignments for ambiguous distance constraints. In the final round, 12 of 50 structures had no violations greater than 0.5 Å. These were used to calculate an average structure. Structures were analyzed using Procheck-NMR (Laskowski et al., 1996) and PROMOTIF (Hutchinson and Thornton, 1996). For the ensemble, 71.7% of the residues were in the most favored regions of the Ramachandran plot, 23.6% were in allowed regions, and 4.8% were in disallowed regions. No constraints were available for residues 2083–2086, and these residues were excluded from the calculation of structural statistics. The average minimized structure was submitted to DALI (Dietmann et al., 2001) to search for homologous domains. Figures were generated using MolScript (Kraulis, 1991), Raster3D (Merritt and Bacon, 1997), Grasp (Nicholls et al., 1991), and InsightII (Molecular Simulations).

CD Spectroscopy

IBiD and TIF-2 were dissolved at 20 μM in 10 mM potassium phosphate (pH 7.0), 50 mM KCl. Experiments were carried out at 20°C on a Jasco Spectrometer with 1 nm resolution, a response time of 8 s and five measurements/data point in tandem cell (Hellma) containing two compartments separated by a quartz window.

Preparation of IBiD-Agarose Beads

Four residues (Cys-Gly-Gly-Ser) were inserted by PCR between the TEV site and IBiD. Cys-tagged IBiD was overexpressed in *E. coli*, purified by Ni-NTA resin, cleaved by TEV protease, and purified by Hi-Trap Q ion exchange chromatography. The protein was fully reduced in 100 mM DTT at 50°C for 30 min, followed by RP-HPLC purification to homogeneity. ESI-MS detected no residual disulfide product. Crosslinking to SulfoLink beads (Pierce, Rockford, IL) was done according to the manufacturer's suggestions, yielding ~0.5 mg protein/mL resin. Control SulfoLink beads were prepared by blocking all crosslinking sites in 100 mM cysteine, 50 mM Tris-HCl, and 5 mM EDTA (pH 8.5).

In Vitro Protein-Protein Interaction Assays

Conditions for GST pull-downs have been described (Falvo et al., 2000). For each reaction using IBiD-agarose, 20 μl of beads (diluted 1:10 with control beads) were used. For competition experiments, the protein complexes were assembled on IBiD-agarose and washed before being challenged by TIF-2 peptide in binding buffer at room temperature for 2 hr. ^{35}S-labeled proteins that remained bound were analyzed by SDS-PAGE.

Transfections and EMSAs

Human endometrial carcinoma cells (HEC-1B) were grown in DMEM containing 10% FBS to 70%–80% confluence. Transfections used LipofectAMINE (Life Technologies) following the manufacturer's instructions. Typically, cells in each 3.5 cm well were transfected with 0.5 μg of reporter, 1 μg of effector, and 0.25 μg of pCMV-LacZ in Opti-MEM (Life Technologies) for 24 hr. Cells were mock- or Sendai virus (SPAFAS)-infected for 16 hr before analysis. Chloramphenicol acetyltransferase activity was normalized to β-galactosidase activity. WCE preparation, binding, and PAGE conditions for EMSA have been described (Wathelet et al., 1998).

Acknowledgments

We thank H. Gronemeyer, P. Pitha, and M. Wathelet for generously providing reagents; E. Woo, A. Fotin, C. Molodowitch, and A. Khederian for help with experimental work; D. King for mass spectrometry; N. Sinitskaya for peptide synthesis; and P. Sliz and U. Unligil for software support. We also thank H. Matsuo, G. Heffron, J. Gross, S. Hyberts, and M. Berardi for assistance with NMR experiments and G. Verdine for use of the CD spectrometer.

This work was supported by NIH grants AI-20642 (to T.M.), GM-47467 (to G.W.), and GM-39589 (to S.C.H.). S.C.H. is an Investigator in the Howard Hughes Medical Institute. E.F. acknowledges a fellowship (DRG 1547) from the Cancer Research Fund of the Damon

Runyon-Walter Winchell Foundation, and B.J.H. acknowledges a fellowship from the Medical Foundation.

Received May 3, 2001; revised July 5, 2001.

References

Ackrill, A.M., Foster, G.R., Laxton, C.D., Flavell, D.M., Stark, G.R., and Kerr, I.M. (1991). Inhibition of the cellular response to interferons by products of the adenovirus type 5 E1A oncogene. Nucleic Acids Res. *19*, 4387–4393.

Archer, S.J., Ikura, M., Torchia, D.A., and Bax, A. (1991). An alternative 3D NMR technique for correlating backbone N-15 with side chain Hβ resonances in larger proteins. J. Magn. Reson. *95*, 636–641.

Austen, M., Luscher, B., and Luscher-Firzlaff, J.M. (1997). Characterization of the transcriptional regulator YY1. J. Biol. Chem. *272*, 1709–1717.

Bartels, C., Xia, T.H., Billeter, M., Guntert, P., and Wuthrich, K. (1995). The program XEASY for computer-supported NMR spectral-analysis of biological macromolecules. J. Biomol. NMR *6*, 1–10.

Berger, S.L. (1999). Gene activation by histone and factor acetyltransferases. Curr. Opin. Cell Biol. *11*, 336–341.

Bordoli, L., Netsch, M., Luthi, U., Lutz, W., and Eckner, R. (2001). Plant orthologs of p300/CBP: conservation of a core domain in metazoan p300/CBP acetyltransferase-related proteins. Nucleic Acids Res. *29*, 589–597.

Brunger, A.T., Adams, P.D., Clore, G.M., DeLano, W.L., Gros, P., Grosse-Kunstleve, R.W., Jiang, J.S., Kuszewski, J., Nilges, M., Pannu, N.S., et al. (1998). Crystallography & NMR system: a new software suite for macromolecular structure determination. Acta Crystallogr. D Biol. Crystallogr. *54*, 905–921.

Bucher, P., Karplus, K., Moeri, N., and Hofmann, K. (1996). A flexible motif search technique based on generalized profiles. Comput. Chem. *20*, 3–24.

Burysek, L., Yeow, W.S., Lubyova, B., Kellum, M., Schafer, S.L., Huang, Y.Q., and Pitha, P.M. (1999). Functional analysis of human herpesvirus 8-encoded viral interferon regulatory factor 1 and its association with cellular interferon regulatory factors and p300. J. Virol. *73*, 7334–7342.

Clore, G.M., Bax, A., and Gronenborn, A.M. (1991). Stereospecific assignment of β-methylene protons in larger proteins using 3D ^{15}N-separated Hartmann-Hahn and ^{13}C-separated rotating frame Overhauser spectroscopy. J. Biomol. NMR *1*, 13–22.

Cornilescu, G., Delaglio, F., and Bax, A. (1999). Protein backbone angle restraints from searching a database for chemical shift and sequence homology. J. Biomol. NMR *13*, 289–302.

De Guzman, R.N., Liu, H.Y., Martinez-Yamout, M., Dyson, H.J., and Wright, P.E. (2000). Solution structure of the TAZ2 (CH3) domain of the transcriptional adaptor protein CBP. J. Mol. Biol. *303*, 243–253.

Deleage, G., and Geourjon, C. (1993). An interactive graphic program for calculating the secondary structure content of proteins from circular dichroism spectrum. Comput. Appl. Biosci. *9*, 197–199.

Dietmann, S., Park, J., Notredame, C., Heger, A., Lappe, M., and Holm, L. (2001). A fully automatic evolutionary classification of protein folds: Dali Domain Dictionary version 3. Nucleic Acids Res. *29*, 55–57.

Falvo, J.V., Parekh, B.S., Lin, C.H., Fraenkel, E., and Maniatis, T. (2000). Assembly of a functional beta interferon enhanceosome is dependent on ATF-2-c-jun heterodimer orientation. Mol. Cell. Biol. *20*, 4814–4825.

Feng, X.H., Zhang, Y., Wu, R.Y., and Derynck, R. (1998). The tumor suppressor Smad4/DPC4 and transcriptional adaptor CBP/p300 are coactivators for Smad3 in TGF-β-induced transcriptional activation. Genes Dev. *12*, 2153–2163.

Giles, R.H., Peters, D.J., and Breuning, M.H. (1998). Conjunction dysfunction: CBP/p300 in human disease. Trends Genet. *14*, 178–183.

Glass, C.K., and Rosenfeld, M.G. (2000). The coregulator exchange in transcriptional functions of nuclear receptors. Genes Dev. *14*, 121–141.

Goodman, R.H., and Smolik, S. (2000). CBP/p300 in cell growth, transformation, and development. Genes Dev. *14*, 1553–1577.

Hottiger, M.O., and Nabel, G.J. (2000). Viral replication and the coactivators p300 and CBP. Trends Microbiol. *8*, 560–565.

Hutchinson, E.G., and Thornton, J.M. (1996). PROMOTIF—a program to identify and analyze structural motifs in proteins. Protein Sci. *5*, 212–220.

Janknecht, R., and Hunter, T. (1996). Versatile molecular glue. Transcriptional control. Curr. Biol. *6*, 951–954.

Janknecht, R., Wells, N.J., and Hunter, T. (1998). TGF-β-stimulated cooperation of Smad proteins with the coactivators CBP/p300. Genes Dev. *12*, 2114–2119.

Jayaraman, G., Srinivas, R., Duggan, C., Ferreira, E., Swaminathan, S., Somasundaram, K., Williams, J., Hauser, C., Kurkinen, M., Dhar, R., et al. (1999). p300/cAMP-responsive element-binding protein interactions with ets-1 and ets-2 in the transcriptional activation of the human stromelysin promoter. J. Biol. Chem. *274*, 17342–17352.

Kraulis, P. (1991). MOLSCRIPT: a program to produce both detailed and schematic plots of protein structures. J. Appl. Crystallogr. *24*, 946–950.

Kumar, K.P., McBride, K.M., Weaver, B.K., Dingwall, C., and Reich, N.C. (2000). Regulated nuclear-cytoplasmic localization of interferon regulatory factor *3*, a subunit of double-stranded RNA-activated factor 1. Mol. Cell. Biol. *20*, 4159–4168.

Kurokawa, R., Kalafus, D., Ogliastro, M.H., Kioussi, C., Xu, L., Torchia, J., Rosenfeld, M.G., and Glass, C.K. (1998). Differential use of CREB binding protein-coactivator complexes. Science *279*, 700–703.

Kussie, P.H., Gorina, S., Marechal, V., Elenbaas, B., Moreau, J., Levine, A.J., and Pavletich, N.P. (1996). Structure of the MDM2 oncoprotein bound to the p53 tumor suppressor transactivation domain. Science *274*, 948–953.

Laskowski, R.A., Rullmannn, J.A., MacArthur, M.W., Kaptein, R., and Thornton, J.M. (1996). AQUA and PROCHECK-NMR: programs for checking the quality of protein structures solved by NMR. J. Biomol. NMR *8*, 477–486.

Lei, M., Lu, W., Meng, W., Parrini, M.C., Eck, M.J., Mayer, B.J., and Harrison, S.C. (2000). Structure of PAK1 in an autoinhibited conformation reveals a multistage activation switch. Cell *102*, 387–397.

Li, M., Damania, B., Alvarez, X., Ogryzko, V., Ozato, K., and Jung, J.U. (2000). Inhibition of p300 histone acetyltransferase by viral interferon regulatory factor. Mol. Cell. Biol. *20*, 8254–8263.

Lin, R., Heylbroeck, C., Pitha, P.M., and Hiscott, J. (1998). Virus-dependent phosphorylation of the IRF-3 transcription factor regulates nuclear translocation, transactivation potential, and proteasome-mediated degradation. Mol. Cell. Biol. *18*, 2986–2996.

Mamane, Y., Heylbroeck, C., Genin, P., Algarte, M., Servant, M.J., LePage, C., DeLuca, C., Kwon, H., Lin, R., and Hiscott, J. (1999). Interferon regulatory factors: the next generation. Gene *237*, 1–14.

Maniatis, T., Falvo, J.V., Kim, T.H., Kim, T.K., Lin, C.H., Parekh, B.S., and Wathelet, M.G. (1998). Structure and function of the interferon-β enhanceosome. Cold Spring Harb. Symp. Quant. Biol. *63*, 609–620.

McKnight, C.J., Matsudaira, P.T., and Kim, P.S. (1997). NMR structure of the 35-residue villin headpiece subdomain. Nat. Struct. Biol. *4*, 180–184.

Merika, M., Williams, A.J., Chen, G., Collins, T., and Thanos, D. (1998). Recruitment of CBP/p300 by the IFN-β enhanceosome is required for synergistic activation of transcription. Mol. Cell *1*, 277–287.

Merritt, E.A., and Bacon, D.J. (1997). Raster3D: photorealistic molecular graphics. Methods Enzymol. *277*, 505–524.

Nakajima, T., Uchida, C., Anderson, S.F., Lee, C.G., Hurwitz, J., Parvin, J.D., and Montminy, M. (1997). RNA helicase A mediates association of CBP with RNA polymerase II. Cell *90*, 1107–1112.

Nguyen, H., Hiscott, J., and Pitha, P.M. (1997). The growing family

of interferon regulatory factors. Cytokine Growth Factor Rev. *8*, 293–312.

Nicholls, A., Sharp, K.A., and Honig, B. (1991). Protein folding and association: insights from the interfacial and thermodynamic properties of hydrocarbons. Proteins *11*, 281–296.

Nilges, M., and O'Donoghue, S. (1998). Ambiguous NOEs and automated NOE assignment. Prog. NMR Spec. *32*, 107–139.

Papoutsopoulou, S., and Janknecht, R. (2000). Phosphorylation of ETS transcription factor ER81 in a complex with its coactivators CREB-binding protein and p300. Mol. Cell. Biol. *20*, 7300–7310.

Parekh, B.S., and Maniatis, T. (1999). Virus infection leads to localized hyperacetylation of histones H3 and H4 at the IFN-β promoter. Mol. Cell *3*, 125–129.

Parker, D., Jhala, U.S., Radhakrishnan, I., Yaffe, M.B., Reyes, C., Shulman, A.I., Cantley, L.C., Wright, P.E., and Montminy, M. (1998). Analysis of an activator:coactivator complex reveals an essential role for secondary structure in transcriptional activation. Mol. Cell *2*, 353–359.

Parker, D., Rivera, M., Zor, T., Henrion-Caude, A., Radhakrishnan, I., Kumar, A., Shapiro, L.H., Wright, P.E., Montminy, M., and Brindle, P.K. (1999). Role of secondary structure in discrimination between constitutive and inducible activators. Mol. Cell. Biol. *19*, 5601–5607.

Patel, D., Huang, S.M., Baglia, L.A., and McCance, D.J. (1999). The E6 protein of human papillomavirus type 16 binds to and inhibits coactivation by CBP and p300. EMBO J. *18*, 5061–5072.

Perissi, V., Dasen, J.S., Kurokawa, R., Wang, Z., Korzus, E., Rose, D.W., Glass, C.K., and Rosenfeld, M.G. (1999). Factor-specific modulation of CREB-binding protein acetyltransferase activity. Proc. Natl. Acad. Sci. USA *96*, 3652–3657.

Radhakrishnan, I., Perez-Alvarado, G.C., Parker, D., Dyson, H.J., Montminy, M.R., and Wright, P.E. (1997). Solution structure of the KIX domain of CBP bound to the transactivation domain of CREB: a model for activator:coactivator interactions. Cell *91*, 741–752.

Sementchenko, V.I., and Watson, D.K. (2000). Ets target genes: past, present and future. Oncogene *19*, 6533–6548.

Sheppard, H.M., Harries, J.C., Hussain, S., Bevan, C., and Heery, D.M. (2001). Analysis of the steroid receptor coactivator 1 (SRC1)-CREB binding protein interaction interface and its importance for the function of SRC1. Mol. Cell. Biol. *21*, 39–50.

Spector, S., Young, P., and Raleigh, D.P. (1999). Nativelike structure and stability in a truncation mutant of a protein minidomain: the peripheral subunit-binding domain. Biochemistry *38*, 4128–4136.

Szyperski, T., Neri, D., Leiting, B., Otting, G., and Wuthrich, K. (1992). Support of ^{1}H NMR assignments in proteins by biosynthetically directed fractional ^{13}C-labeling. J. Biomol. NMR *2*, 323–334.

Thanos, D., and Maniatis, T. (1995). Virus induction of human IFN-β gene expression requires the assembly of an enhanceosome. Cell *83*, 1091–1100.

Torchia, J., Rose, D.W., Inostroza, J., Kamei, Y., Westin, S., Glass, C.K., and Rosenfeld, M.G. (1997). The transcriptional co-activator p/CIP binds CBP and mediates nuclear receptor function. Nature *387*, 677–684.

Uesugi, M., Nyanguile, O., Lu, H., Levine, A.J., and Verdine, G.L. (1997). Induced α helix in the VP16 activation domain upon binding to a human TAF. Science *277*, 1310–1313.

Van Orden, K., Giebler, H.A., Lemasson, I., Gonzales, M., and Nyborg, J.K. (1999). Binding of p53 to the KIX domain of CREB binding protein. A potential link to human T-cell leukemia virus, type I-associated leukemogenesis. J. Biol. Chem. *274*, 26321–26328.

Voegel, J.J., Heine, M.J., Tini, M., Vivat, V., Chambon, P., and Gronemeyer, H. (1998). The coactivator TIF2 contains three nuclear receptor-binding motifs and mediates transactivation through CBP binding-dependent and -independent pathways. EMBO J. *17*, 507–519.

Wathelet, M.G., Lin, C.H., Parekh, B.S., Ronco, L.V., Howley, P.M., and Maniatis, T. (1998). Virus infection induces the assembly of coordinately activated transcription factors on the IFN-β enhancer in vivo. Mol. Cell *1*, 507–518.

Xu, W., Doshi, A., Lei, M., Eck, M.J., and Harrison, S.C. (1999). Crystal structures of c-Src reveal features of its autoinhibitory mechanism. Mol. Cell *3*, 629–638.

Accession Numbers

The coordinates of the IBiD structure have been deposited in the Protein Data Bank under ID code 1JJS.